The 2021 World Congress on
Advances in Structural Engineering and Mechanics (ASEM21)
GECE, Seoul, Korea, August 23-26, 2021

Effect of Plastic Deformation on the Martensitic Transformations in TiNi Alloy

*Margarita E. Evard[1)], Fedor S. Belyaev[2)], Aleksandr E. Volkov[3)]

[1) 3)] *Department of Mathematics and Mechanics, Saint Petersburg State University, Universitetskaya Nab. 7-9, St. Petersburg, 199034, Russia*
[2)] *Laboratory of Mathematical Methods in Mechanics of Materials, Institute for Problems in Mechanical Engineering, V.O., Bolshoj pr. 61, St. Petersburg, 199178, Russia*
[1)] *m.evard@spbu.ru*

ABSTRACT

A model of plastic deformation of the shape memory alloys which describes dislocation slip at the microlevel is developed. A condition similar to the Schmid law was adopted for the determination of dislocation slip onset. A description of the interaction of plastic deformation and martensitic transformations by taking into account the densities of deformation defects is proposed. It is shown that the model can correctly describe the effect of plastic strain on the shape memory effect. The proposed model is also capable of describing the two-way shape memory effect.

1. INTRODUCTION

Plastic shear is not only one of deformation mechanisms of a shape memory alloy (SMA) but also plays an important role in the formation of its functional properties. The dislocation slip is responsible for the formation of the two-way shape memory effect and for the "training" of the material. Thus, plastic deformation can be used to purposefully improve of the SMA properties. Therefore it is difficult to overestimate the importance of taking into account the effect of plastic deformation when creating SMA applications. Unfortunately it is impossible to describe in a simple way all the features of the influence of this deformation on the SMA functional properties. In this regard, there is a need for specific calculation tools that would make it possible to describe both the plastic deformation itself and its effect on the SMA functional properties.

In this study, we will distinguish the irreversible deformation: caused by external forces, which we will call active plastic deformation, and the deformation caused by internal stresses and securing the accommodation of martensite plates, which we will call microplastic deformation. The most promising from the point of view of a wide

---

[1)] Corresponding author, Ph.D., Assistant professor
[2)] Ph.D., Senior researcher
[3)] D.Sci., Professor

description of the SMA functional properties are microstructural models. Models of this class are based on the concept of multilevel development of deformation and averaging of microstrains. Early microstructural models (Likhachev 1995, Patoor 1996, Volkov 1996, Gao 2000, Huang 2000) were developed to describe only reversible phase deformation. However, they could not describe the entire range of phenomena associated with martensitic transformations. The earliest models describing microplastic deformation were (Sun 1996, Evard 1999, Volkov 2002, Evard 2006). They introduced internal variables that are measures of microplastic deformations associated with each of the martensite variants. In the work (Sun 1996), it was assumed that microplastic deformation increases with the motion of the interphase boundaries. In works (Evard 1999, Volkov 2002, Evard 2006), conditions similar to the flow conditions in the one-dimensional case with isotropic hardening were proposed to describe microplastic deformation. In the work (Manchiraju 2010), a microstructural finite element model was proposed that describes phase transformations and microplastic deformation. To describe a polycrystalline sample, a finite element model of a representative cubic volume was built, divided into equal cubic elements, which are grains with different orientations of crystallographic axes. Such a choice of a representative volume made it possible to take into account the internal stresses arising from the incompatibility of grain strains. The most recent works on microstructural modeling of SMA include works (Yu 2012, 2013, 2014, 2015). In the work (Yu 2012), a model is presented that describes the superelastic behavior of a polycrystalline sample. Its feature is the use of an explicit self-consistency scheme to describe the interaction of the grains that make up the sample, which does not require a lot of calculations. The works (Yu 2013, 2014, 2015) represent the further development of this model and offer descriptions of various deformation mechanisms of the SMA, including microplastic and active plastic deformation. Despite the significant development of microstructural models, they do not describe the effect of active plastic deformation on martensitic transformations.

A previously developed microstructural model (Belyaev 2015, 2018, 2019) was that able to describe the main SMA functional properties and the microplastic deformation. The effect of microplastic deformation on the martensite transformation process was taken into account by introducing into the model internal variables that describe the stresses arising during the growth of martensite plates. The purpose of this work was to describe active plastic deformation and its effect on phase transformations in SMA within the framework of the microstructural model.

2. MODEL

The description of the SMA plastic deformation in this work is based on the authors previously developed model (Belyaev 2015, 2018, 2019). In the proposed microstructural approach the strain of SMA representative volume is calculated by describing various deformation mechanisms at the micro-level followed by averaging the strains of micro-volumes. Consideration of different structural levels in the model makes possible accounting for the structure of the material.

2.1 Structural levels and strain averaging

The subject of the description is the representative volume, which is the material point of the specimen. It is considered that the representative volume consists of grains, which in turn consist of domains of austenite and orientation variants of martensite.
Small strain tensors are used. To calculate the strain at the macro-level, the Reuss' hypothesis is applied: the strain ε of the representative volume is found by averaging the strains ε^{gr} of the grains constituting the representative volume. Grains have various orientations ω of the crystallographic axes and averaging is performed over all orientations:

$$\varepsilon = \sum_{\omega} f(\omega)\varepsilon^{gr}(\omega), \tag{1}$$

where $f(\omega)$ is the volume fraction of grains with orientation ω. The strain of each grain is found as the sum of micro-strains obtained from various deformation mechanisms:

$$\varepsilon^{gr} = \varepsilon^{e} + \varepsilon^{T} + \varepsilon^{Ph} + \varepsilon^{MP} + \varepsilon^{P} . \tag{2}$$

Elastic ε^e, thermal $\boldsymbol{\varepsilon}^T$, phase $\boldsymbol{\varepsilon}^{Ph}$, microplastic $\boldsymbol{\varepsilon}^{MP}$ and active plastic strain $\boldsymbol{\varepsilon}^P$ are taken into account. Elastic and thermal strains are found in the common way according to Hook's law and the law of thermal expansion. To describe the phase strain, internal variables Φ_n are introduced in the model, such that Φ_n/N is the volume fraction of the n-th Bain's variant of martensite in the grain; N is the number of the crystallographically equivalent variants of martensite. The total volume fraction of martensite Φ^{gr} in a grain and the phase strain of the grain $\boldsymbol{\varepsilon}^{Ph}$ are calculated as:

$$\Phi^{gr} = \frac{1}{N}\sum_{n=1}^{N}\Phi_n , \tag{3}$$

$$\varepsilon^{Ph} = \frac{1}{N}\sum_{n=1}^{N}\Phi_n D^n , \tag{4}$$

where D_n is the tensor of the Bain's deformation for the n-th variant of martensite.

2.2 Martensite transformation description

Thermodynamic forces determining the process of the martensitic transformation, i.e. the evolution of the internal variables Φ_n are obtained as derivatives of the Gibbs' potential G. This potential for one grain of the two-phase material can be split into the eigenpotential G^{eig} and the potential of mixing G^{mix}:

$$G = G^{eig} + G^{mix} . \tag{5}$$

The eigenpotential is the potential of non-interacting austenite and martensite and is given by relations (see for example Volkov 2001):

$$G^{eig} = (1 - \Phi^{gr})G^{A} + \frac{1}{N}\sum_{n=1}^{N}\Phi_n G^{Mn} , \tag{6}$$

$$G^{a} = G_0^a - S_0^a(T - T_0) - \frac{c_\sigma^{0a}(T-T_0)^2}{2T_0} - \varepsilon_{ij}^{0Ta}(T)\sigma_{ij} - \frac{1}{2}Q_{ijkl}^{a}\sigma_{ij}\sigma_{kl} , \qquad a = A, Mn , \tag{7}$$

where T_0 is the temperature of the thermodynamic equilibrium of austenite and martensite at zero stress, G_0^a and S_0^a are the values of the Gibbs' potential and of the entropy at $T = T_0$ and $\sigma = 0$, c_σ^a is the specific heat (per unit volume), $\varepsilon^{0a}(T)$ is the strain at $\sigma = 0$, Q^a is the tensor of elastic compliances.

The mixing potential corresponds to the elastic energy of the internal stresses caused by the incompatibilities of the phase deformation. Its correct calculation is a very complicated task demanding the knowledge of the particular configuration of the martensite Bain's domains and plates as well as of the boundary conditions on the internal boundaries. This model exploits the same idea as in (Niclaeys 2002) and the mixing potential is approximated by a quadratic form:

$$G^{mix} = \frac{\mu}{2}\sum_{m,n=1}^{N} A_{mn}(\Phi_m - b_m)(\Phi_n - b_n)\,. \tag{8}$$

In (8) new internal variables b_n are introduced. They stand for the oriented deformation defects densities, caused by the internal stresses and reducing the elastic energy of the inter-phase interaction. Material constants μ and A_{mn} describe the magnitude of the interaction as well as the preference of the appearance of the particular combinations of the martensite Bain's variants. An estimation of the values of these constants for TiNi was considered in (Volkov 2015). From Eqs. (5-8) the thermodynamic forces for the martensitic transformation are derived as:

$$F_n = -\frac{\partial G}{\partial \Phi_n} \approx \frac{q_0(T-T_0)}{T_0} + D_{ij}^n \sigma_{ij} - \mu\sum_{m=1}^{N} A_{mn}(\Phi_m - b_m)\,, \tag{9}$$

were q_0 is latent heat (enthalpy) of the direct martensitic transformation.

In the terms of the thermodynamic forces F_n the condition of the transformation of austenite into the n-th variant of martensite can be formulated as:

$$F_n = \pm F^{fr}\,, \tag{10}$$

where F^{fr} is the dissipative force describing the hysteresis of the martensitic transformation (the deviation of the force F_n from the thermodynamic equilibrium $F_n = 0$); the plus sign in (10) is for the direct and minus is for the reverse transformation.

2.3 Microplastic deformation description

Microplastic strains are caused by the incompatibility of the phase deformation. The main assumption for its calculation is that the phase strain of a Bain's variant activates a combination of slips producing a strain proportional to the deviator of the phase strain. Thus, the microplastic strain can be calculated as follows:

$$\varepsilon^{gr\,MP} = \frac{1}{N}\sum_{n=1}^{N} \kappa\varepsilon_n^{mp} dev(D^n)\,, \tag{11}$$

where ε_n^{mp} are microplastic strains related to the n-th variant of martensite, κ is scaling factor for microplastic strain.

To find the variation of microplastic strains ε_n^{mp} we formulate the flow conditions in the form:

$$\left|F_n^p - F_n^\rho\right| = F^y\,, \quad \left(F_n^p - F_n^\rho\right)dF_n^p > 0\,, \tag{12}$$

where F_n^p is the generalized force conjugated with the parameters b_n:

$$F_n^p = -N\frac{\partial G}{\partial b_n} = \mu\sum_{m=1}^{N} A_{mn}(\Phi_m - b_m)\,. \tag{13}$$

The forces F^y and F_n^ρ are responsible for isotropic and kinematic hardening. The formulated microplastic flow condition is analogous to the classical flow condition in the one-dimensional case. The force F_n^p plays the role of stress and F^y and F_n^ρ the roles of the flow stress and the back stress respectively.

Deformation defects generated by the micro plastic flow we divide in two groups: oriented defects b_n generating long-range stress fields and scattered defects f, suggesting the evolution equations for them in the form:

$$\dot{b}_n = \dot{\varepsilon}_n^{mp} - \frac{1}{\beta^*}|b_n|\dot{\varepsilon}_n^{mp}H\left(b_n\dot{\varepsilon}_n^{mp}\right)\,, \tag{14}$$

$$\dot{f} = \sum_{m=1}^{N}\left|\dot{\varepsilon}_n^{mp}\right| + r_1(f - f_0)\dot{\Phi}_M H\left(-\dot{\Phi}_M\right)\,, \tag{15}$$

where β^* is maximum value of the oriented defects density, r_1 is scattered defects healing factor, f_0 is initial value of scattered defects, H is the Heaviside function.

For the closing equations that connect the density of deformation defects with hardening the simplest linear form is chosen:

$$F_n^\rho = a_\rho b_n\,, \tag{16}$$

$$F^y = a_y f\,, \tag{17}$$

where a_ρ and a_y are the kinematic and isotropic hardening factors.

2.4 Plastic deformation description

To describe active plastic deformation within the framework of a microstructural model, it is necessary to formulate the constitutive relations of this process at the micro level – for a single grain. As a rule, in metals and alloys, dislocation slip occurs only on several specific crystallographic planes. For other systems, the realization of plastic shears is difficult because of the yield stress for these planes is greater than the ultimate strength of the material.

Any slip plane can be attributed to one of families, each consisting of K_m crystallographically equivalent planes, numbered 1, ..., k, ..., K_m. For example, in the austenitic B2 phase of TiNi SMA slip occurs on the planes belonging to two families: {110} and {100}, first consisting of 6 and the second of 3 planes. Plastic deformation ε_ω^{grp} in grain ω is the sum of deformations in each of the shear planes belonging to this grain:

$$\dot{\varepsilon}_{\omega}^{gr\,p} = \sum_{m=1}^{M} \sum_{k=1}^{Km} \dot{\varepsilon}_{\omega}^{p(m,k)}\,, \tag{18}$$

where $\varepsilon_{\omega}^{p(m,k)}$ is the deformation carried out by shear in the *k*-th plane from the *m*-th family.

In each slip plane we introduce a local basis, such that its 3-d axis is normal to the plane and the 1-st and the 2-nd axes lie in the plane. We assume that the only components of the stress related to this local basis, which produce slip on this plane are $\tau_{31}^{(m,k)}$ and $\tau_{32}^{(m,k)}$. Let σ^{gr} be the effective stress applied to the grain. Then, in consistence with the Reuss' hypothesis these two components are found by the formulae:

$$\begin{aligned} \tau_{31}^{(m,k)} &= A_{p3}^{(m,k)} A_{q1}^{(m,k)} \sigma_{pq}^{gr}\,, \\ \tau_{32}^{(m,k)} &= A_{p3}^{(m,k)} A_{q2}^{(m,k)} \sigma_{pq}^{gr}\,, \end{aligned} \tag{19}$$

where A_{pq} is the rotation matrix that transforms the crystallophysic basis of the grain ω into the local basis associated with the plane *(m,k)*.

The condition for the onset of the plastic shear is formulated as the Schmid law: plastic flow begins when the shear component of the stress $\tau_{31}^{(m,k)}$ or $\tau_{32}^{(m,k)}$ reaches a critical value τ^{s} for the given slip system:

$$\tau^{s\,(m,k)} = \begin{cases} \tau_{31}^{(m,k)}\,, & if\ \tau_{31}^{(m,k)} \geq \tau_{32}^{(m,k)} \\ \tau_{32}^{(m,k)}\,, & if\ \tau_{31}^{(m,k)} < \tau_{32}^{(m,k)} \end{cases} \tag{20}$$

In this case, deformation accumulates in the admissible shear direction. The components of shear deformation are $\beta_{31}^{(m,k)}$ and $\beta_{32}^{(m,k)}$ on the plane *(m, k)*.

We assume that the flow stress $\tau^{s(m,k)}$ is the sum of the initial (equilibrium) value $\tau^{s(m,k)}{}_{eq}$ which is the same for all planes belonging to the given *m*-th group, and the addition $\tau^{s(m,k)}{}_{def}$ responsible for the strain hardening:

$$\tau^{s(m,k)} = \tau_{eq}^{s(m,k)} + \tau_{def}^{s(m,k)}\,. \tag{21}$$

To calculate the value of $\tau^{s(m,k)}{}_{def}$ we assume that the strain hardening coefficient *h(m)* does not depend on the shear value, thus the $\tau^{s(m,k)}{}_{def}$ growth rate is:

$$\dot{\tau}_{def}^{s(m,k)} = \begin{cases} h\left|\dot{\beta}_{31}^{(m,k)}\right|, & if\ \left|\dot{\beta}_{31}^{(m,k)}\right| > 0 \\ h\left|\dot{\beta}_{32}^{(m,k)}\right|, & if\ \left|\dot{\beta}_{32}^{(m,k)}\right| > 0 \end{cases} \tag{22}$$

The plastic deformation of the grain $\varepsilon_{\omega}^{gr\,p}$ is determined using the summation (18), and the macroscopic plastic deformation ε^{p} is determined by averaging over all the grains of the representative volume.

2.5 Plastic deformation and martensitic transformation interaction

Plastic deformation causes generation of deformation defects, for example dislocations. Pile-ups of these defects generate long-range stress fields in the material and, therefore, they are the sources of internal stresses, which contribute to the effective stress applied to the grain, and thus affect the martensitic transformation. In a similar way, the martensitic transformation is affected by microplastic deformation, which arises due to the incompatibility of deformations near the boundaries of growing martensite plates.

The deformation defects produced by the microplastic deformation are taken into account by the densities of these defects b_n generated by the growth of each of 1, ..., *n,* ..., *N* variants of martensite. The influence of the densities b_n on the martensitic transformation is taken into account in the mixing potential (8). Since the physical nature of plastic and microplastic deformations is the same (dislocation shear) and they generate the same defects (ensembles of dislocations), it must be possible to express the densities of the defects associated with the plastic deformation in terms of the densities of the defects associated with the microplastic deformation. Thus, the effect of plastic deformation on the martensitic transformation will be taken into account.

To characterize the deformation defects associated with the plastic deformations $\beta_{31}^{(m,k)}$ and $\beta_{32}^{(m,k)}$ of the *(m,k)* slip system variables $b_1^{(m,k)}$ and $b_2^{(m,k)}$ are introduced. Evolution equations from (Volkov 2015) similar to Eq. (14) for microplastic deformation are used for calculation of their values:

$$\begin{aligned}\dot{b}_1^{(m,k)} &= \dot{\beta}_{31}^{a(m,k)} - \frac{\left|b_1^{(m,k)}\right|}{\beta^*}\dot{\beta}_{31}^{a(m,k)} H\left(\dot{\beta}_{31}^{a(m,k)} b_1^{(m,k)}\right),\\ \dot{b}_2^{(m,k)} &= \dot{\beta}_{32}^{a(m,k)} - \frac{\left|b_2^{(m,k)}\right|}{\beta^*}\dot{\beta}_{32}^{a(m,k)} H\left(\dot{\beta}_{32}^{a(m,k)} b_2^{(m,k)}\right),\end{aligned} \tag{23}$$

where β^* is the maximum value of the defects density.

Variables $b_1^{(m,k)}$ and $b_2^{(m,k)}$ can be viewed as components of the vector $b^{(m,k)}$ which characterizes defects of *(m,k)* slip system in the local basis of the shear plane. In this basis $b_3^{(m,k)}$ is always equal to zero since the plastic shear is parallel to the slip plane. Therefore the tensor of internal stresses generated by deformation defects of slip system *(m,k)* can be introduced as b_n where *n* is the normal vector to the corresponding slip plane. Since vectors *b* and *n* are perpendicular to each other than tensor b_n is a deviator and it can be expressed in coordinates of Ilyushin's five-dimensional deviatorial space (Ilyushin 1990). Its basis tensor in this study are taken in the form:

$$\begin{aligned}U_1 &= \sqrt{\frac{2}{3}}\left(e_1 e_1 - \frac{1}{2}e_2 e_2 - \frac{1}{2}e_3 e_3\right),\\ U_2 &= \frac{1}{\sqrt{2}}(e_2 e_2 - e_3 e_3),\\ U_3 &= \frac{1}{\sqrt{2}}(e_1 e_2 + e_2 e_1),\\ U_4 &= \frac{1}{\sqrt{2}}(e_2 e_3 + e_3 e_2),\\ U_5 &= \frac{1}{\sqrt{2}}(e_3 e_1 + e_1 e_3),\end{aligned} \tag{24}$$

where e_1, e_2, e_3 are the basis vectors of the crystallographic coordinate system of the grain.

Summing up the internal stresses of all slip systems, we obtain tensor *B*, which we call the effective field of defects. Its coordinates B_i in the basis (24) are as follows:

$$B_i = \sum_{m,k}(n^{mk} b^{mk}) : U_i \, . \tag{25}$$

The effective field of defects determines the internal stresses in the grain generated by active plastic deformation. It also makes it possible to take into account the effect of these stresses on martensitic transformations. The contribution of active plastic deformation defects to the stress fields of microplastic deformation can be obtained by the equation:

$$b_n = \sum_i B_i U_i : (dev(D^n))^{-1} \, . \tag{26}$$

With Eqs. (23)–(26), the contribution of plastic deformation defects to the Gibbs' potential is calculated and, thus, an account of the effect of plastic deformation on the martensitic transformations is made.

3. SIMULATION RESULTS

An equiatomic TiNi alloy was chosen as a model material. This alloy is quite popular and widely used in applications. It is known that the plastic shear in TiNi alloy occurs in two systems of planes: {100} and {110} (Chowdhury 2017). Therefore, to describe the plastic deformation, it is necessary to choose the constants for both slip systems. Fitted material constants for the model material are presented in Table 1.

To test the capabilities of the model in describing the SMA plastic deformation a number of numerical experiments were carried out on the TiNi alloy straining at different temperatures. In order to ensure the implementation of the mechanism of active plastic deformation in each experiment, the straining was carried out up to 20%. This value of strain exceeds the theoretical capabilities of the phase deformation of the TiNi alloy and at the same time does not lead to its fracture. The test temperatures were chosen so as to provide different initial states of the alloy: martensite, austenite, high-temperature state when force initiation of martensitic transformations is impossible (also austenite).

Table 1 Material constants for TiNi alloy.

Material constant	Symbol	Value
Number of martensite variants	*N*	12
Latent heat of the direct martensitic transformation	q_0	-160 MJ/m^3
Characteristic temperatures	*Mf*	329 K
	Ms	337 K
	As	357 K
	Af	371 K

Temperature of the thermodynamic equilibrium	T_0	354 K
Micro plastic strain scaling factor	κ	7
Isotropic hardening factor	a_y	2 MPa
Kinematic hardening factor	a_ρ	50 MPa
Maximum value of the defects density	β^*	0.013
Initial value of scattered defects	f_0	5
Scattered defects healing factor	r_1	$8 \cdot 10^{-5}$
Initial yield stress for {100} slip system	$\tau^{s\,eq}_{\{100\}}$	85 MPa
Hardening coefficient for {100} slip system	$h^{\{100\}}$	100 MPa
Initial yield stress for {110} slip system	$\tau^{s\,eq}_{\{110\}}$	100 MPa
Hardening coefficient for {110} slip system	$h^{\{110\}}$	3000 MPa

Fig. 1 (a) shows the deformation curve of the TiNi alloy at a temperature of 600 K, which is higher than the *Md* temperature (i.e., a temperature above which force initiation of the martensitic transformation is impossible). At this temperature, the material is in a high-temperature austenitic state. In segment 1-2, the alloy is deformed elastically, at point 2 it reaches the yield point, and then deforms plastically 2-3. Unloading 3-4 occurs according to the elastic law. After unloading, significant residual deformation is observed, since deformation mainly occurred due to the active plastic deformation.

On the Fig. 1 (b) the diagram of a TiNi alloy straining at a temperature of 400 K is presented. This temperature is slightly above of the end of the reverse martensite transformation (*Af* = 371 K) and below the *Md* temperature. At these conditions, the alloy is also in the austenitic state, but there is a possibility of force initiation of the martensitic transformation. In segment 1-2, the alloy is deformed elastically. At point 2, a phase transformation begins due to the applied stress and therefore in segment 2-3 the slope of the curve decreases. At point 3, the material reaches the yield limit and in segment 3-4, the mechanism of active plastic deformation acts. Unloading occurs first according to the elastic law in segment 4-5, then in segment 5-6 the reverse martensitic transformation occurs with the recovery of strain (the effect of superelasticity) and elastic unloading continues in segment 6-7. After unloading a residual strain is observed due to the mechanisms of active plastic and microplastic deformations. The residual strain in this case is less than after straining at a temperature of 600 K because here it is partially restored due to the realization of the superelasticity effect.

On the Fig. 1 (c) the diagram of a TiNi alloy straining at a temperature of 300 K is presented. This temperature is lower than the end of the direct martensite transformation (*Mf* = 329 K). At this temperature, the material is fully in the martensitic state. In segment 1-2 the alloy is deformed elastically. Then at point 2 it reaches the twinning limit and a reorientation of martensite occurs during segment 2-3. At the same time, the volume fractions of martensite variants that provide tensile strain increases due to a decrease in the volume fraction of the remaining variants. At point 3, the possibilities of material deformation due to the reorientation of martensite are exhausted and in segment 3-4 it is deformed mainly elastically. At point 4, the material reaches the yield limit and in segment 4-5 it deforms plastically. Unloading occurs at first elastically 5-6, and at the end with some reverse reorientation of martensite 6-7.

The strain at point 7 is the sum of the phase, active plastic and microplastic strains. In order to separate the strain of the plastic mechanisms, the material is heated to the austenitic state (segment 7-8). After heating, the phase strain is restored (shape memory effect) and at point 8, residual plastic strain is observed. This strain is also less than in Fig 1 (a), since part of the strain was obtained due to phase transformations.

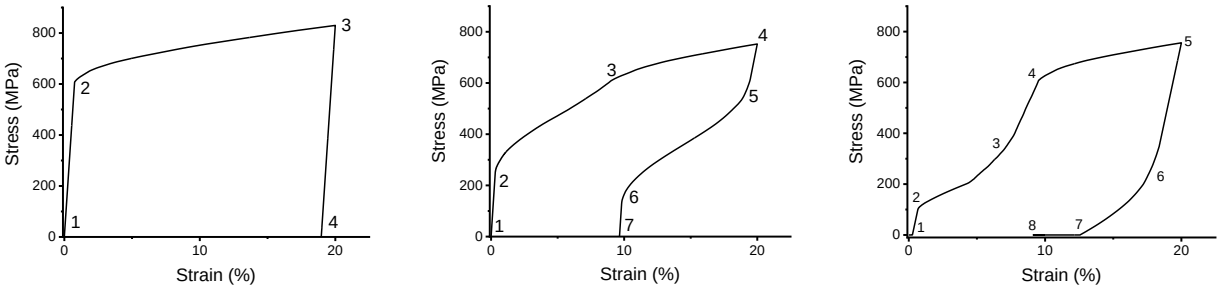

(a) *(b)* *(c)*

Fig.1 Deformation curves of TiNi alloy at temperature 600 K (a), 400 K (b), 300 K (c).

To test the model, experimental data were taken from work (Belyaev 2006) illustrating the effect of plastic strain on the martensitic transformations in TiNi alloy. In the work (Belyaev 2006) a number of experiments were carried out according to the scheme shown on the Fig. 2 Straining of the sample in the austenitic state (0-1) was carried out at 600 K, so that only the dislocation slip was activated. Plastic deformation was carried out in the torsion mode and the residual strain after unloading (1-2) varied within 2-30%. After plastic deformation the sample was transformed into the martensitic state (3-2) by cooling down to the room temperature, deformed (3-4) to the residual strain $\gamma_r \approx 3\%$ and unloaded (4-5). Subsequent heating (5-6) and cooling (6-7) of the sample allowed measuring the strain recovery. Using the developed model, similar numerical experiments were carried out.

The capacity of the body to recover the strain on heating was characterized by the factor of strain recovery K equal to the ratio of the recovered strain to the strain imparted to the body in the martensitic state: $K = (\gamma_{sm}/\gamma_r)$ where γ_{sm} is the shape memory effect strain. The simulated and experimental dependences of K versus the value of the preliminary plastic strain are presented on the Fig. 3.

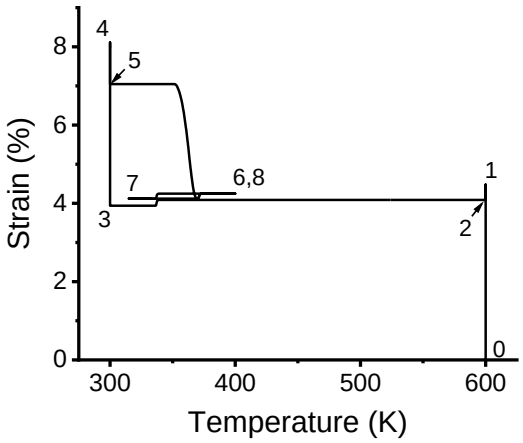

Fig. 2 Experiment scheme on the strain – temperature plane.

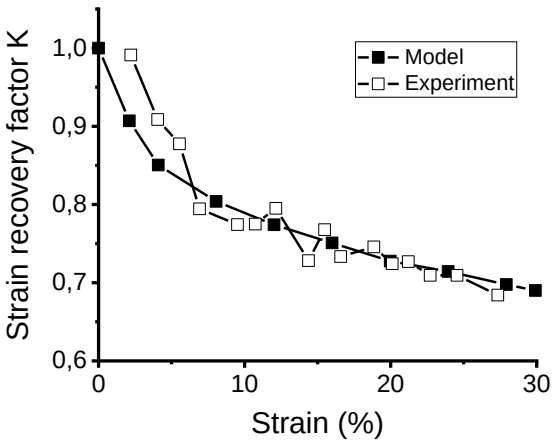

Fig. 3 Strain recovery factor on the value of the preliminary plastic strain.

The Fig. 3 shows that the strain recovery factor *K* decreases with preliminary plastic strain growth. As noted in work (Belyaev 2006) a decrease of *K* is associated with the formation of the effect of two-way shape memory (TWSM) effect during plastic straining of the sample in the high-temperature austenitic state. The TWSM effect on heating gives a strain of the opposite sign to shape memory strain, which is responsible for shape recovery, and thus to a decrease in *K*. The same conclusions can be drawn from the analysis of model curves. On the Fig. 2 one can see the implementation of TWSM effect as a small loop (6-7-8) during cooling and heating without applied stress. The dependence of the strain value of TWSM on preliminary plastic deformation is shown on the Fig. 4.

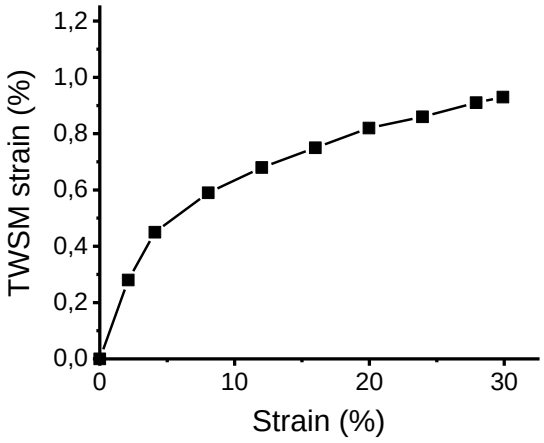

Fig. 4 Two-way shape memory effect strain on the value of the preliminary plastic strain.

In this way it can be concluded that the developed model makes it possible to correctly describe the development of internal stresses that affect martensitic transformations through the calculation of deformation defects of plastic deformation. In addition, the accuracy of the model is confirmed by the capacity to describe the TWSM effect, since its implementation is directly related to the development of certain fields of internal stresses.

4. CONCLUSIONS

As a result of the present work a model of SMA plastic deformation was developed based on a microstructural approach. Consideration of the shear at the microlevel makes possible describing the plastic deformation of the SMA representative volume. Taking into account the densities of the deformation defects produced by active plastic deformation allows describing its effect on the martensitic transformations. A satisfactory description of the effect the of preliminary plastic strain of the TiNi alloy in austenitic state on the shape memory strain is reached. A correct description of the internal stress fields also makes possible describing the effect of two-way shape memory.

ACKNOWLEDGMENTS

The reported study was funded by RFBR, projects 19-31-60035 and 19-01-00685.

REFERENCES

Belyaev, F.S., Evard, M.E., Volkov, A.E. and Volkova, N.A. (2015), “A microstructural model of SMA with microplastic deformation and defects accumulation: application to thermocyclic loading”, *Mater. Today: Proc.*, **2**(suppl. 3), S583–S587.

Belyaev, F.S., Volkov, A.E. and Evard, M.E. (2018), "Microstructural modeling of fatigue fracture of shape memory alloys at thermomechanical cyclic loading", *AIP Conf. Proc.*, **1959**, 070003.

Beliaev, F.S., Evard, M.E., Ostropiko, E.S., Razov, A.I. and Volkov, A.E. (2019), "Aging Effect on the One-Way and Two-Way Shape Memory in TiNi-Based Alloys", *Shape Memory and Superelasticity*, **5**(3), 218–229.

Belyaev, S.P., Resnina, N.N. and Volkov, A.E. (2006), "Influence of irreversible plastic deformation on the martensitic transformation and shape memory effect in TiNi alloy", *Mater. Sci. Eng.: A*, **438–440**, 627–629.

Chowdhury, P. and Sehitoglu, H. (2017), "A revisit to atomistic rationale for slip in shape memory alloys", *Progress in Mater. Sci.*, **85**, 1–42.

Evard, M.E. and Volkov, A.E. (1999), "Modeling of martensite accommodation effect on mechanical behavior of shape memory alloys", *J. Eng. Mater. Technol.*, **121**(1), 102–104.

Evard, M.E., Volkov, A.E. and Bobeleva, O.V. (2006), "An approach for modelling fracture of shape memory alloy parts", *Smart Structures and Systems*, ***2***(4), 357–363.

Gao, X., Huang, M. and Brinson, L.C. (2000), "A multivariant model for SMAs Part 1. Crystallographic issues for single crystal model", *Int. J. Plasticity*, **16**(10-11), 1345–1369.

Huang, M., Gao, X. and Brinson, L.C. (2000), "A multivariant micromechanical model for SMAs, Part 2. Polycrystal model", *Int. J. Plasticity*, **16**(10-11), 1371–1390.

Ilyushin, A.A. (1990), *Continuum Mechanics*, Moscow State University, Moscow, Russia. (in Russian)

Likhachev, V.A. (1995), "Structure-analytical theory of martensitic unelasticity", *J. Phys. IV*, **05**(C8), 137–142.

Manchiraju, S. and Anderson, P.M. (2010), "Coupling between martensitic phase transformations and plasticity: A microstructure-based finite element model", *Int. J. Plasticity*, **26**(10), 1508–1526.

Niclaeys, C., Ben Zineb, T., Arbab-Chirani, S. and Patoor, E. (2002), "Determination of the interaction energy in the martensitic state", *Int. J. Plasticity*, **18**(11), 1619–1647.

Patoor, E., Eberhardt, A. and Berveiller, M. (1996), "Micromechanical modelling of superelasticity in shape memory alloys", *J. Phys. IV*, **06**(C1), 277–292.

Sun, Q.-P. and Lexcellent, C., (1996), "On the unified micromechanics constitutive description of one-way and two-way shape memory effects", *J. Phys. IV*, **06**(C1), 367–375.

Volkov, A.E., Evard, M.E., Kurzeneva, L.N., Likhachev, V.A., Sacharov, V,Yu. and Ushakov, V.V. (1996), "Mathematical modeling of martensitic inelasticity and shape memory effects", *J. Tech. Phys.*, **66**(11), 3–34. (in Russian)

Volkov, A.E. and Casciati, F. (2001), "Simulation of dislocation and transformation plasticity in shape memory alloy polycrystals", *Shape memory alloys. Advances in modelling and applications*, Auricchio, F., Faravelli, L., Magonette, G., Torra, V., Eds., CIMNE, Barcelona, 88–104.

Volkov, A.E. (2002), "Microstructural modeling of deformation of alloys during repeated martensitic transformations", *Izv. Academy of Sciences. Ser. Phys.*, **66**(9), 1290–1297. (in Russian)

Volkov, A.E., Belyaev, F.S., Evard, M.E. and Volkova, N.A. (2015), "Model of the evolution of deformation defects and irreversible strain at thermal cycling of stressed TiNi alloy specimen", *MATEC Web Conf.*, **33**, 03013.

Yu, C., Kang, G., Song, D. and Kan, Q. (2012), "Micromechanical constitutive model considering plasticity for super-elastic NiTi shape memory alloy", *Computational Mater. Sci.*, **56**, 1–5.

Yu, C., Kang, G., Kan, Q. and Song, D. (2013), "A micromechanical constitutive model based on crystal plasticity for thermo-mechanical cyclic deformation of NiTi shape memory alloys", *Int. J. Plasticity*, **44**, 161–191.

Yu, C., Kang, G. and Kan, Q. (2014), "Crystal plasticity based constitutive model of NiTi shape memory alloy considering different mechanisms of inelastic deformation", *Int. J. Plasticity*, **54**, 132–162.

Yu, C., Kang, G., Song, D. and Kan, Q. (2015), "Effect of martensite reorientation and reorientation-induced plasticity on multiaxial transformation ratchetting of super-elastic NiTi shape memory alloy: New consideration in constitutive model", *Int. J. Plasticity*, **67**, 69–101.